Geophysical Research Letters

RESEARCH LETTER
10.1029/2018GL080793

Role of Arctic Sea Ice in the 2014–2015 Eurasian Warm Winter

Jinbo Xie[1], **Minghua Zhang**[2,3], **and Hailong Liu**[1,4]

[1]State Key Laboratory of Numerical Modeling for Atmospheric Sciences and Geophysical Fluid Dynamics, Institute of Atmospheric Physics, Chinese Academy of Sciences, Beijing, China, [2]School of Marine and Atmospheric Sciences, State University of New York at Stony Brook, Stony Brook, NY, USA, [3]International Center for Climate and Environment Sciences, Institute of Atmospheric Physics, Chinese Academy of Sciences, Beijing, China, [4]College of Earth Sciences, University of Chinese Academy of Sciences, Beijing, China

Key Points:
- Anomalous Barents Sea ice contributed to significant shift in skewness for the 2014-2015 winter warming over the Eurasian continent
- Barents Sea ice exhibits asymmetric forcing on the Eurasian continent circulation depending on the atmospheric state
- Persistence of the sea ice anomaly is important for this forcing of the climate and weather patterns in regions south of the Arctic

Supporting Information:
- Supporting Information S1
- Data Set S1

Correspondence to:
J. Xie,
xiejinbo@mail.iap.ac.cn

Citation:
Xie, J., Zhang, M., & Liu, H. (2019). Role of Arctic sea ice in the 2014–2015 Eurasian warm winter. *Geophysical Research Letters*, *46*, 337–345. https://doi.org/10.1029/2018GL080793

Received 6 OCT 2018
Accepted 22 DEC 2018
Accepted article online 3 JAN 2019
Published online 10 JAN 2019

Abstract Because of large internal variabilities, the role of Arctic sea ice concentration (SIC) on regional climate cannot be easily separated. This study uses two groups of large ensemble atmospheric model simulations under climatological and observed SIC boundary conditions to investigate the role of SIC in the 2014–2015 December to February Eurasian warm winter (DJF15). It is shown that the SIC has large impact on the probability distribution function of the DJF15 temperature and pressure fields. The anomalous high Barents Sea ice during the 2014–2015 autumn and winter leads to significant shift in the probability distribution function skewness of the DJF15 surface temperature (from −0.13 to −0.48) and the related sea level pressure (from −0.18 to 0.32) that favor more occurrences of warm temperature anomaly and positive North Atlantic Oscillation-like pattern. This asymmetry is consistent with anomalous forcing in phase with the anomalies of the sea level pressure field.

Plain Language Summary Anomalous Arctic sea ice regulates heat exchanges between the ocean and atmosphere, thereby modifying the equator-pole temperature gradient and affecting the atmospheric circulation and weather patterns at southern latitudes. In this study, we utilize large ensemble numerical simulations to investigate the role of Arctic sea ice on the Eurasian warm winter in 2014–2015. Our analysis shows that the sea ice forcing shifts the skewness of the simulated event-related temperature and sea level pressure, resulting in asymmetrical forcing on the related sea level pressure depending on the atmospheric state. These results emphasize the importance of analyzing beyond the mean and variance in fully characterizing sea ice forcing on atmosphere, which are essential for regional weather pattern prediction and climate risk assessments.

1. Introduction

Changes in sea ice in the Arctic substantially modify heat and water fluxes between the sea surface and atmosphere, consequently influencing the atmosphere above this region. The related changes in the equator-pole temperature gradient arising from varying sea ice cover, along with changes in the transport of heat and moisture between lower and higher latitudes, can result in a speeding up or slowing down of the jet stream, which can cause decrease or increase in temperature and precipitation in the midlatitude region (Cvijanovic & Caldeira, 2015; Francis & Vavrus, 2012; Liu et al., 2012; Overland & Wang, 2010). Thus, investigations into the role of Arctic sea ice in regional extremes is of significance for understanding potential changes in extreme weather and climate events.

The potential remote impact of Arctic sea ice change on wintertime cooling and warming over the midlatitude continent has been addressed previously (Blunden & Arndt, 2016; Cassano & Cassano, 2017; Inoue et al., 2012; Liu et al., 2012; Mori et al., 2014; Yang et al., 2016). The link between changes in Arctic sea ice coverage and extreme events could have major socioeconomic impacts, but uncertainties about the significance and robustness of these signals remain, with some studies showing a weak or no influence of Arctic sea ice change (Barnes, 2013; Li et al., 2015; Screen et al., 2013). One important uncertainty arises from the strong internal atmospheric variability that often camouflages the circulation response to sea ice (Screen et al., 2014). The probability density function (PDF) analysis, including the skewness of atmospheric variability, can be used to evaluate changes in weather and climate risk related to sea ice concentration (SIC) while taking internal atmospheric variability into account. Skewness describes the asymmetry of the PDF

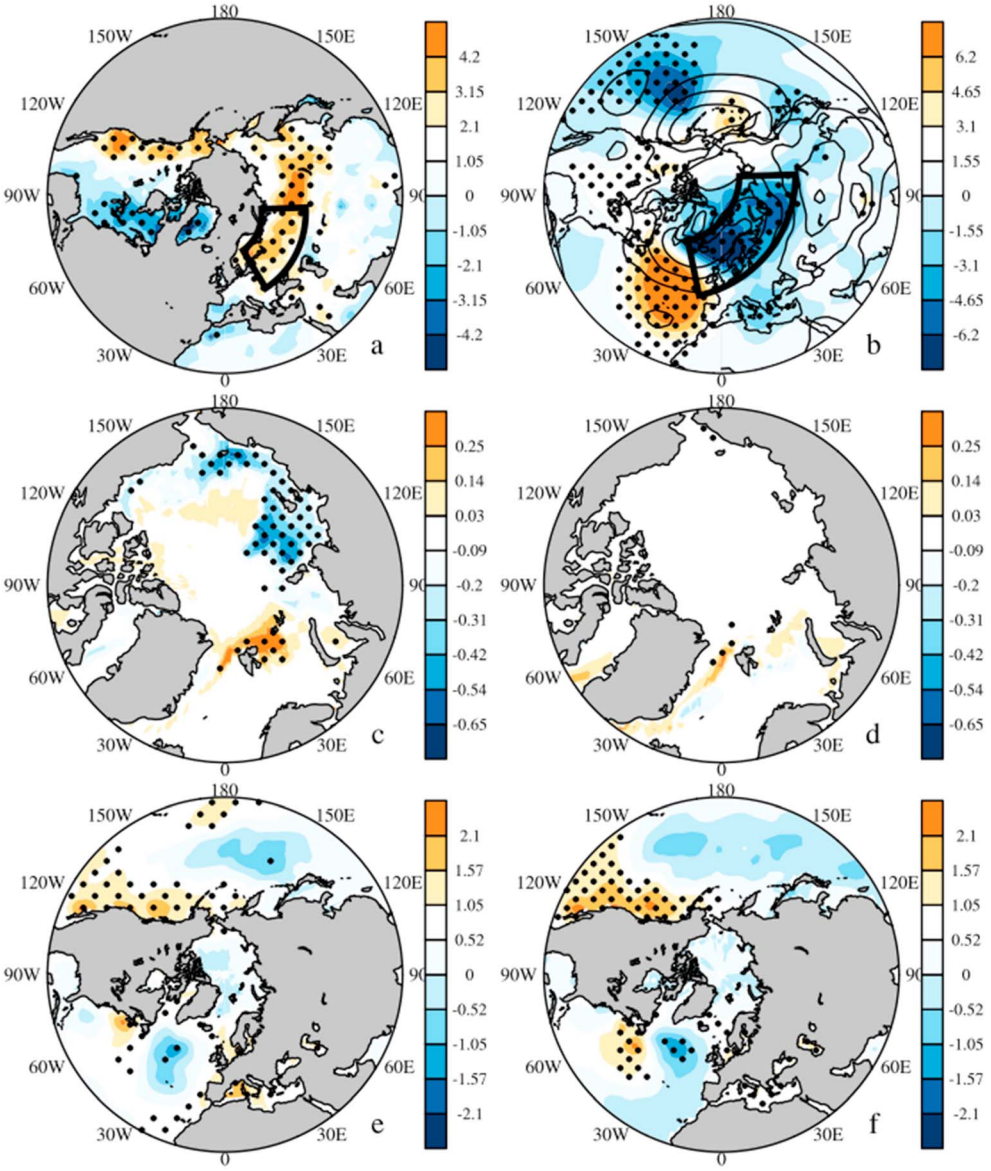

Figure 1. The 2014–2015 winter observational anomalies of (a) monthly 2-m air temperature (K), (b) sea level pressure (hPa) from NCEP-DOE II, and the autumn-winter observational anomalies of (c, d) sea ice from Hadley Center SIC sea ice concentration and (e, f) sea surface temperatures from sea surface temperatures compiled by Hurrell et al. (2008). The anomalies are relative to the 1979–2012 climatological mean. The overlay contour in (b) is the observed sea level pressure climatological mean. The dots denote the areas that passed the 90% significance test. The black boxes in (a) and (b) denote the SIBTEMP and the SIBPSL region used to define the event.

where positive skewness refers to distribution that "lean" to the left—mass of the distribution is concentrated on the left of the mean and a longer right tail, and the opposite for negative skewness. This statistic has often been used to characterize the non-Gaussian behavior of the atmosphere that has been identified for features such as highly nonlinear regime behavior (Majda et al., 2006; Sura & Hannachi, 2015). The possible link between the recent reduction in Arctic sea ice changes and the wintertime North Atlantic Oscillation (NAO) using skewness was discussed by Nakamura et al. (2015).

The Eurasian continent experienced an extreme warm season during the 2014–2015 winter (Blunden & Arndt, 2016). A strong warm band spanned the whole Russia region (Figure 1a), causing a series of repeatedly record-breaking temperatures registered in many cities, including Moscow, St. Petersburg, Tambov, Voronezh, Tomsk, and Kemerovo (Blunden & Arndt, 2016). This pattern was also captured in the extreme

warm temperatures recorded (defined by the warmest 90 daily days in December–February) with the anomalous high temperature of 3~4° compared with other years (Figure S1a). Accompanying the temperature pattern was a signal of positive NAO (Figure 1b), which produced warmer and more moist advection over the northern Eurasian continent. This positive NAO pattern was seen more clearly in the 500-hPa geopotential height (Figure S1b) despite the fact that it extended less over the Eurasian continent, indicating the low-level feature of the warm and moist advection generated by the circulation. This circulation was also associated with the second wettest winter since 1935 (Blunden & Arndt, 2016) and anomalous high rain-on-snow events, which, along with the warming, can lead to large ecological and social impacts, such as increasing thaw of permafrost, induced slush avalanches, and closing of roads and airports caused by significant ground-ice cover (Blunden & Arndt, 2016; Hansen et al., 2014; Pavol, 2014; Screen & Simmonds, 2012).

Here we report a set of modeling experiments designed to assess the influence of Arctic sea ice forcing on the Eurasian 2014–2015 anomalous winter warming (DJF15). We evaluated changes in the PDF of the DJF15 temperature and that of related sea level pressure (SLP) associated with sea ice change using two large ensemble simulations with perturbed initial conditions and specified observed global sea surface temperatures (SST) and two SIC forcings: a control run with observed SIC forcing and a comparison run with climatological SIC. A *k*-means cluster analysis was used to corroborate the PDF analysis. In addition, three experiments using climatological, observed, and doubled Barents Sea SIC anomalies were used to verify the robustness of the SIC forcing effect and to generalize the results to every year.

2. Model, Experiment Design, and Method

Version 4 of the Community Atmospheric Model (CAM4), which has a finite volume dynamical core (Neale et al., 2010) and an active Community Land Model version 4 (Lawrence et al., 2011), was used to conduct the simulations. SST and SIC were used in data-driven mode. All of the CAM4 and Community Land Model version 4 simulations were carried out using a nominal 1° (0.9° × 1.25°) latitude-longitude horizontal resolution with 26 vertical layers. The monthly evolving SST and SIC climatological values were taken from the SST and SIC catalog (1979–2012) compiled by Hurrell et al. (2008), and the SST and SIC anomaly data are taken respectively from SST catalog by Hurrell et al. (2008) and the Hadley SIC catalog (Rayner et al., 2003).

The experiments comprised an Atmospheric Model Intercomparison Project integration that was used as a reference, and two ensembles of 100 short-term simulations from 2014 July to 2015 March using observed SST and two SIC values, one with the observed SIC (ALL) and the other using monthly climatological SIC (CLIM-SIC, 1979 to 2012 average). The 100 short-term simulations differed only in their initial conditions and were formed by using fields in two randomly selected years in the 50 consecutive days from 6 June to 25 July in a 20-year simulation with climatological SST and SIC. To verify the effect of the 2014–2015 autumn to winter Barents Sea ice, we ran three additional sets of 100-year sequential experimental tests with climatological SST and varied SIC forcing: climatological SIC (1979–2012, CTRL-run), Barents Sea and nearby region (60 N–90 N, 25 W-90E) anomalous high ice from 2014 to 2015 July to March (1xBarents-run), and doubled Barents Sea and nearby region anomalous high ice (2xBarents-run). The April–June SIC forcing were set to climatological SIC, and the SST forcing was altered following Cassano et al. (2014) to avoid physical inconsistency between the SST and SIC.

All anomalies in the above experiments were calculated using the period relative to the 1979–2012 period in the Atmospheric Model Intercomparison Project simulation. To define the DJF15 event, we used the area average of the DJF15 region temperature and the associated SLP (denoted as SIBTEMP for temperature region and SIBPSL for SLP region in the black box indicated in Figures 1a and 1b, respectively). The PDFs of the ensembles were derived using the SIBTEMP temperature and SIBPSL SLP index and was smoothed using an Epanechnikov kernel (Epanechnikov, 1969). To compare the ensemble mean results against observation, the observed temperatures and SLP anomalies were taken from the National Centers for Environmental Prediction, Department of Energy Reanalysis 2 (Kanamitsu et al., 2002), for the reference period of 1979–2012.

The skewness parameter was used in the comparison of the PDFs. It describes the asymmetry of a PDF: positive skewness means the mass of the distribution is concentrated on the left of the mean and a longer right tail. The opposite is true for negative skewness. We calculated the skewness parameters following Sura & Hannachi (2015). The Student's *t* test was used to determine the statistical significance of the difference in

the mean of two ensembles, and a bootstrap subsampling method was used to determine the statistical significance in the difference of the skewness parameters between the two ensembles following Berg et al. (2014). The 90% significance level was used for the Student's *t* test. As for the bootstrap method, the two ensembles being compared were concatenated, shuffled randomly, and redrawn 10,000 times, with the difference in skewness estimated to be significant when greater than (lower) than the 95% (5%) percentile of the corresponding distribution of differences.

To corroborate our PDF analysis on the DJF15 event, we used the *k*-means cluster analysis method following Xie & Zhang (2017) on the CLIM-SIC and ALL simulation Eurasian (20–160°E, 20–75°N) SLP anomaly ensemble members. We focused on *k*-means of the SLP because this SLP region spans a larger area and, thus, it was easier to separate between the different regimes of the DJF15-related circulation. In performing the cluster analysis, we weighted the data by the square root of the cosine of latitude so that the variance at each data point was weighted in accordance with the area that it represented. We chose a cluster number *k* of 4 after comparing the occurrence frequency of the observed-like clusters (defined as members for which the SIBPSL weighted area average did not exceed −1.75 hPa) for both simulations (Figure S2), which showed a consistently higher but similar difference in ALL compared with CLIM-SIC.

3. Results

The observed SIC and SST are shown in Figures 1c–1f. The anomalous SIC from autumn to winter in 2014–2015 showed an anomalous low SIC in the Laptev Sea in autumn that diminished in winter but a persistent anomalous high SIC in the Barents Sea from autumn to winter (Figures 1c and 1d). The SST showed a persistent warm anomaly along the west coast of the United States and a dipole in the North Atlantic from autumn to winter (Figures 1e and 1f).

Under the same observed SIC and SST forcing, the differences among the simulated ensemble members are caused by internal variability, and the anomalous property of the ensemble mean are attributed to the SIC and SST anomalies. Even though the ensemble mean temperature shows a warm temperature pattern (Figure 2a) in the west of the Northern Russia region that partly resembles observation (Figure 1a), consistent with the weak anomalous low SLP structure extending from west Europe to the Norwegian sea (Figure 2b), the magnitudes of both the temperature and pressure patterns are weak, indicating that the anomalous SIC and SST boundary conditions from autumn to winter did not force the core of the DJF15 event.

The anomalous SIC and SST however had a role in altering the probability of such an extreme event. The PDFs of the 100 members of the 2-m temperature and SLP from ALL and CLIM-SIC experiments are shown in Figure 2c (SIBTEMP 2-m temperature) and Figure 2d (SIBPSL SLP), and the annotation above each graph denotes the mean, standard deviation, and the skewness parameters for each PDF. Although the difference between the means and standard deviations are not significant, there are significant shifts in the skewness (as tested by bootstrap test) from the CLIM-SIC to ALL in the SIBTEMP 2-m temperature (from −0.13 to −0.48) and SIBPSL SLP (from −0.18 to 0.32). These shifts indicate asymmetrical forcing of the SIC on the SIBTEMP temperature and SIBPSL SLP, with more frequent occurrence of warm temperature event consistent with the more frequent negative SIBPSL (e.g., positive NAO-like) pattern that promotes warm and moist advection, and less frequent but colder extremes with a less frequent positive SIBPSL (e.g., negative NAO-like) pattern that are of larger amplitudes.

This shift in the regional PDF skewness can be qualitatively corroborated by the *k*-means cluster analysis of the Eurasian region SLP members (Figure 3), where the cluster in the two left columns shows reinforcing of positive NAO phase and diminishing of negative NAO phases (Figures 3a, 3b, 3e, and 3f) from CLIM-SIC to ALL. Accompanying this shift is the amplified negative NAO phases. By contrast, the two clusters in the two right columns that contain >50% of the full members and qualitatively similar in pattern generally remain unchanged in terms of the cluster frequency (Figures 3c, 3d, 3g, and 3h).

The shift in skewness from CLIM-SIC to ALL implies asymmetric SIC forcing on the atmosphere depending on the background state. This dependence can be seen in the difference of the surface energy fluxes and the response of SLP in the low SIBPSL and high SIBPSL members taken separately from ALL and CLIM-SIC. Under the low SIBPSL, the SIC forcing caused energy loss in the Barents Sea and open water region south

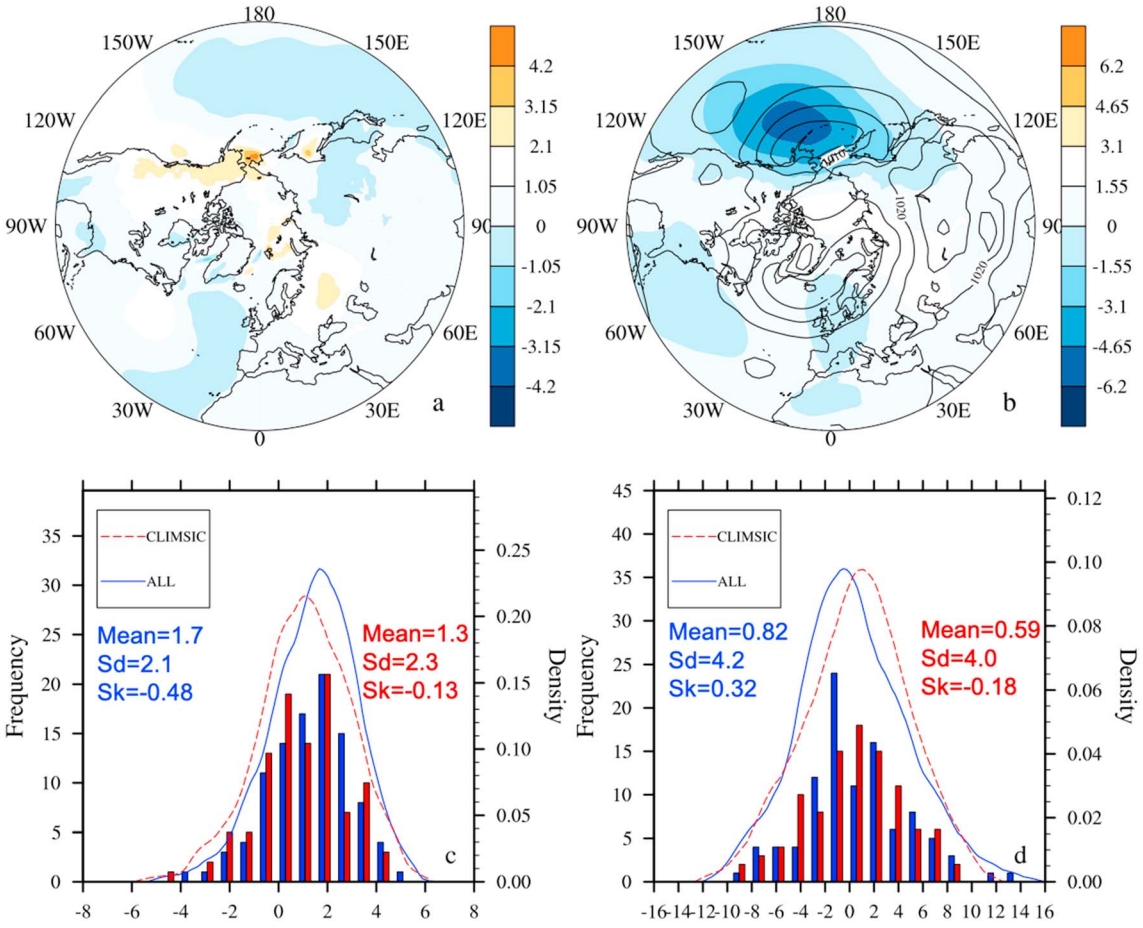

Figure 2. Ensemble mean anomaly of ALL (a) 2-m temperature (K) and (b) sea-level pressure (hPa), and probability distribution function of the 2014–2015 winter ensemble simulation for (c) SIBTEMP 2-m temperature anomaly (K) and (d) SIBPSL sea level pressure (hPa) anomaly of ALL (blue) and CLIM-SIC (red). The anomalies are relative to the 1979–2012 climatological mean of the Atmospheric Model Intercomparison Project simulation. The overlay contour in (b) is the observed sea level pressure climatological mean. The probability distribution function was smoothed using the Epanechnikov kernel. The legends in (c) and (d) indicate the values of the moments of the corresponding distribution: mean, standard deviation (Sd), and skewness (Sk). SIC = sea ice concentration.

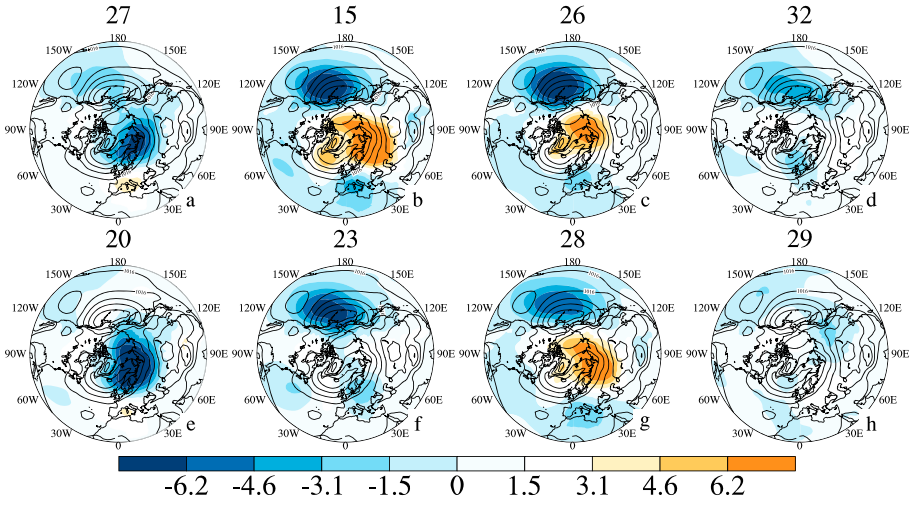

Figure 3. Sea level pressure anomaly clusters of (a–d) ALL and (e–h) CLIM-SIC for $k = 4$. The number above the clusters denotes the number of ensemble members in each cluster. The overlay contour in (a–h) is the observational 1979–2012 sea level pressure climatological mean. The cluster analysis was applied to the Eurasian region (20–160°E, 20–75°N). SIC = sea ice concentration.

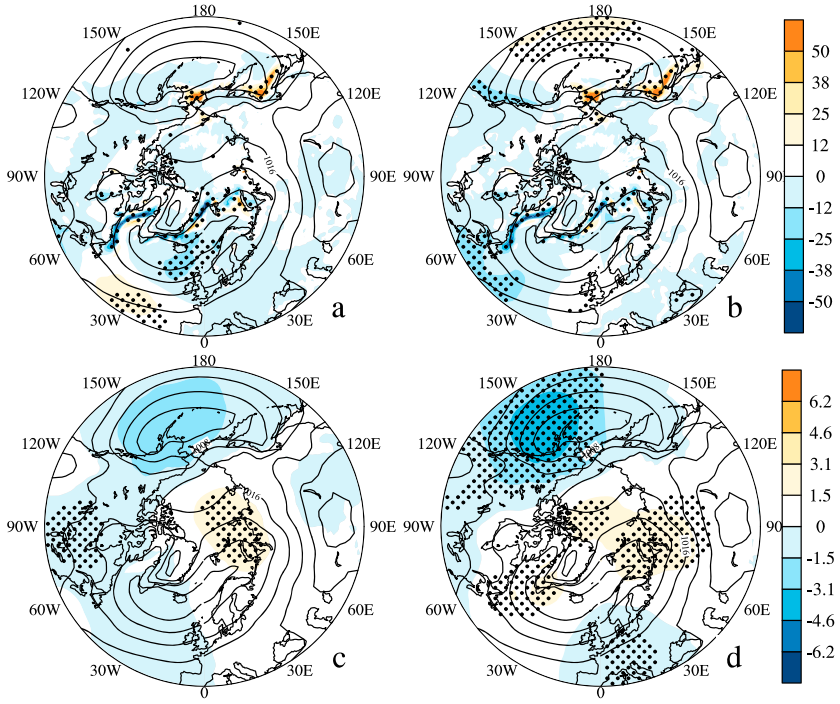

Figure 4. Differences of total energy flux (W/m^2) and sea level pressure (hPa) for ALL (prescribed observed SST and SIC) minus CLIM-SIC (prescribed observed SST and climatological SIC) ensemble members under (a, c) anomalous low SIBPSL sea level pressure and (b, d) anomalous high SIBPSL sea level pressure. The energy terms include surface net shortwave radiation, surface net longwave radiation, sensible heat, and latent heat; upward is positive. The anomalies are relative to the 1979–2012 climatology. The overlay contour is the observational 1979–2012 sea level pressure climatological mean. The dots in (a–d) denote areas that passed the 90% significance test. SST = sea surface temperatures; SIC = sea ice concentration.

of the Greenland upstream of the Eurasian continent (Figure 4a). This energy loss is out of phase with the low SIBPSL SLP field and caused an anomalous zonally oriented surface high east of the climatological trough (Figure 4c). Under high SIBPSL, however, the SIC forcing caused energy loss in the Barents Sea upstream of the Eurasian continent (Figure 4b). This energy loss along with that in the Labrador Sea is in phase with the high SIBPSL SLP field and is associated with the near-resonant amplification of the two-wave anomalous SLP structure in the midlatitude region. This amplification pattern includes an anomalous meridional-oriented surface high that extends far into the Eurasian continent (Figure 4d) associated with the upstream Barents Sea ice forcing. The low-SIBPSL energy loss is in accordance with the "cold arctic-warm continent" surface temperature pattern in the Eurasian sector (Figures S3a and S3b) that is associated with the anomalous surface low near the Russian coast (Figures S3e and S3f), thus reinforcing this thermal forcing and favoring the occurrence of more zonal near-surface circulation in the Eurasian sector; under high-SIBPSL, however, the energy loss is in opposite phase with the "warm arctic-cold continent" surface temperature pattern in the Eurasian sector (Figures S3c and S3d) that is associated with the anomalous high (Figures S3g and S3h) and tend to reduce this thermal forcing, thus making formation of the more meridional near-surface circulation in the Eurasian continent more difficult—allowing only the more intense meridional circulation to occur. This dependence of the SIC forcing on the atmosphere background state noted above resembles the nonlinear shift between high and low index flow as a function of meridional temperature gradient shown in Huang et al. (2017) using a conceptual model originally developed by Charney and DeVore (1979). It is necessary to note that although the anomalous energy flux exchange in Barents and Laptev Seas both existed in autumn (Figure S4), winter energy flux change persisted in the Barents Sea and diminished in the Laptev Sea (Figures 4a and 4b), consistent with the anomalous SIC pattern this winter. This indicates the importance of persistent SIC forcing on the atmosphere, which was also indicated in Cassano & Cassano, 2017).

Thus far, we have shown that the Barents Sea ice change can affect the PDF and make an asymmetrical effect on the DJF15 event depending on the atmospheric state. To test the robustness of this Barents Sea ice forcing on atmosphere against SST forcing, we used the additional experiments of a Ctrl, 1xBarents, and 2xBarents run to redraw the temperature and SLP PDF along similar lines to that in Figures 2c and 2d (Figure S5). The SST forcing was set to climatology (average of 1979–2012) in the additional experiments and the difference of 1xBarents run and Ctrl reflect Barents SIC forcing under climatological SST. The 2xBarents run is a sensitivity test of atmospheric response to SIC anomaly amplitude. PDF in the SIBTEMP and SIBPSL variables in the three experiments shows similar shifts in skewness as seen in Figures 2c and 2d. These shifts in skewness scaled linearly with the amplitude in Barents SIC forcing amplitude (from −0.19 to −0.40 to −0.63 for SIBTEMP and from 0.02 to 0.22 to 0.45 for SIBPSL), thus indicating the robustness of this relationship. The above results highlight the importance in analyzing the changes in the higher moments beyond mean and variance in forecast and attribution study of midlatitude weather and climate extremes on seasonal scale, which has been an important topic in the recent year (Simmonds, 2018). The changes in the midlatitude regional weather and climate PDF would have significant consequences for weather and climate risk assessments using *k*-means forecast, as also shown by Xie & Zhang (2017). Under observed DJF15 Barents SIC forcing, the presence of the first cluster and second cluster cannot be neglected (Figures 3a and 3b). The increased probability would make the first cluster event more likely to happen, whereas the second cluster can create strong cold events that extend into the continent despite its lower frequency. This also highlights the importance of improving the Barents "hot spot" in the sea ice distribution forecast that has been an ongoing effort in collaboration programs such as the Study of Environmental Arctic Change. The improved sea ice forecast skill in these regions will benefit the probability forecast of future regional climates that was shown to be under large uncertainty because of internal variability (Deser et al., 2012; Deser & Phillips, 2009; Screen et al., 2013; Shepherd, 2014).

4. Discussion and Conclusions

In this study, we examined the role of Arctic SIC anomalies in the DJF15 Eurasian warm winter event. We conducted two large ensembles of simulations using CAM4 under specified SST and two SIC boundary conditions—one with observed SIC forcing and another with climatological forcing. It was found that persistent Barents SIC forcing from autumn to winter significantly shifted the skewness of the DJF15 regional (SIBTEMP) temperature (from −0.13 to −0.48) and (SIBPSL) SLP (from −0.18 to 0.32) that favors the occurrence of positive temperature anomaly and positive NAO-like patterns. This asymmetric effect of SIC forcing was shown to be dependent on the atmospheric state: a more frequent zonal-oriented near-surface circulation under positive NAO-like state that favors warm events and a less frequent meridional-oriented near-surface circulation under negative NAO-like state that favors cold events in the Eurasian continent. The marginal sea ice forcing had a nonnegligible effect on a seasonal scale, and the Barents should be targeted as a high-priority area to improve weather and seasonal forecasts.

The uncertainties of the above conclusions might arise from our assumption of perfectly predicted SST and SIC, the number of ensemble members, and the single-model structure. Another important fact is that we only considered the first-order "direct" atmospheric response to Arctic sea ice change. The prescribed SIC excluded potential modulation of remote factors such as the Gulf Stream warm SST shown in Figure 1d that may induce moist transport under certain circulation regime and affect the Barents SIC (hence its atmospheric response; Luo et al., 2017; Simmonds & Govekar, 2014). This may affect the Arctic climate aloft through ways such as promoting long-living blocking events (Screen et al., 2012; Luo, Lixin, et al., 2018; Luo, Chen, et al., 2018) and contribute to significant changes in the downward longwave radiation (Lee et al., 2017). Further examinations using coupled models are needed to investigate these issues.

Acknowledgments
We thank Zhenghui Xie, Juanxiong He, Xiaocong Wang, and Yongkun Xie for providing useful advice when writing this paper. We also thank the two anonymous reviewers for their helpful comments on the manuscript. This research is supported by grant 2016YFB0200800 from the National Major Research High Performance Computing Program of China and grant 41806034 from the National Science Foundation of China. Additional support was provided by the Biological and Environmental Research Division in the Office of Sciences of the U.S. Department of Energy (DOE) and by National Science Foundation to the Stony Brook University. NCEP_Reanalysis 2 data were provided by the NOAA/OAR/ESRL PSD, Boulder, Colorado, USA, from their Web site at https://www.esrl.noaa.gov/psd/. The sea surface temperature data catalog from Hurrell et al. (2008) can be obtained from https://svn-ccsm-inputdata.cgd.ucar.edu/trunk/inputdata/. The Hadley sea ice data set can be obtained from their website at https://www.metoffice.gov.uk/hadobs/hadisst/. Data supporting the conclusions (for Figures 2–4) can be obtained from supporting information Data Set S1.

References

Barnes, E. A. (2013). Revisiting the evidence linking Arctic amplification to extreme weather in midlatitudes. *Geophysical Research Letters*, *40*, 4734–4739. https://doi.org/10.1002/grl.50880

Berg, A. M., Lintner, B. R., Findell, K. L., Malyshev, S., Loikith, P. C., & Gentine, P. (2014). Impact of soil moisture-atmosphere interactions on surface temperature distribution. *Journal of Climate*, *27*(21), 7976–7993. https://doi.org/10.1175/JCLI-D-13-00591.1

Blunden, J., & Arndt, D. S. (2016). State of the climate in 2015. *Bulletin of the American Meteorological Society*, *97*(8), Si–S275. https://doi.org/10.1175/2016BAMSStateoftheClimate.1

Cassano, E. N., & Cassano, J. J. (2017). Atmospheric response to anomalous autumn surface forcing in the Arctic Basin. *Journal of Geophysical Research: Atmospheres*, *122*, 9011–9023. https://doi.org/10.1002/2017JD026765

Cassano, E. N., Cassano, J. J., Higgins, M. E., & Serreze, M. C. (2014). Atmospheric impacts of an Arctic sea ice minimum as seen in the Community Atmosphere Model. *International Journal of Climatology*, *34*(3), 766–779. https://doi.org/10.1002/joc.3723

Charney, J. G., & DeVore, J. G. (1979). Multiple flow equilibria in the atmosphere and blocking. *Journal of the Atmospheric Sciences*, *36*(7), 1205–1216. https://doi.org/10.1175/1520-0469(1979)036<1205:MFEITA>2.0.CO;2

Cvijanovic, I., & Caldeira, K. (2015). Atmospheric impacts of sea ice decline in CO_2 induced global warming. *Climate Dynamics*, *44*(5-6), 1173–1186. https://doi.org/10.1007/s00382-015-2489-1

Deser, C., Knutti, R., Solomon, S., & Phillips, A. S. (2012). Communication of the role of natural variability in future North American climate. *Nature Climate Change*, *2*(11), 775–779. https://doi.org/10.1038/nclimate1562

Deser, C., & Phillips, A. S. (2009). Atmospheric circulation trends, 1950–2000: The relative roles of sea surface temperature forcing and direct atmospheric radiative forcing. *Journal of Climate*, *22*(2), 396–413. https://doi.org/10.1175/2008JCLI2453.1

Epanechnikov, V. A. (1969). Non-parametric estimation of a multivariate probability density. *Theory of Probability and its Applications*, *14*(1), 153–158. https://doi.org/10.1137/1114019

Francis, J. A., & Vavrus, S. J. (2012). Evidence linking Arctic amplification to extreme weather in mid-latitudes. *Geophysical Research Letters*, *39*, L06801. https://doi.org/10.1029/2012GL051000

Hansen, B. B., Isaksen, K., Benestad, R. E., Kohler, J., Pedersen, Å. Ø., Loe, L. E., et al. (2014). Warmer and wetter winters: Characteristics and implications of an extreme weather event in the high Arctic. *Environmental Research Letters*, *9*(11), 114,021. https://doi.org/10.1088/1748-9326/9/11/114021

Huang, J., Xie, Y., Guan, X., Li, D., & Ji, F. (2017). The dynamics of the warming hiatus over the Northern Hemisphere. *Climate Dynamics*, *48*(1-2), 429–446. https://doi.org/10.1007/s00382-016-3085-8

Hurrell, J. W., Hack, J. J., Shea, D., Caron, J. M., & Rosinski, J. (2008). A new sea surface temperature and sea ice boundary data set for the Community Atmosphere Model. *Journal of Climate*, *21*(19), 5145–5153. https://doi.org/10.1175/2008JCLI2292.1

Inoue, J., Hori, M. E., & Takaya, K. (2012). The role of Barents Sea ice in the wintertime cyclone track and emergence of a warm-Arctic cold-Siberian anomaly. *Journal of Climate*, *2012*(25), 2561–2568.

Kanamitsu, M., Ebisuzaki, W., Woollen, J., Yang, S.-K., Hnilo, J. J., Fiorino, M., & Potter, G. L. (2002). NCEP-DOE AMIP-II reanalysis (R-2). *Bulletin of the American Meteorological Society*, *83*(11), 1631–1644. https://doi.org/10.1175/BAMS-83-11-1631

Lawrence, D. M., Oleson, K. W., Flanner, M. G., Thornton, P. E., Swenson, S. C., Lawrence, P. J., et al. (2011). Parameterization improvements and functional and structural advances in version 4 of the Community Land Model. *Journal of Advances in Modeling Earth Systems*, *3*, M03001. https://doi.org/10.1029/2011MS000045

Lee, S., Gong, T., Feldstein, S. B., Gong, T., Feldstein, S. B., Screen, J. A., & Simmonds, I. (2017). Revisiting the cause of the 1989–2009 Arctic surface warming using the surface energy budget: Downward infrared radiation dominates the surface fluxes. *Geophysical Research Letters*, *44*, 10,654–10,661. https://doi.org/10.1002/2017GL075375

Li, C., Stevens, B., & Marotzke, J. (2015). Eurasian winter cooling in the warming hiatus of 1998–2012. *Geophysical Research Letters*, *42*, 8131–8139. https://doi.org/10.1002/2015GL065327

Liu, J., Curry, J. A., Wang, H., Song, M., & Horton, R. M. (2012). Impact of declining Arctic sea ice on winter snowfall. *Proceedings of the National Academy of Sciences of the United States of America*, *109*(11), 4074–4079. https://doi.org/10.1073/pnas.1114910109

Luo, B., Lixin, W., Luo, D., Dai, A., & Simmonds, I. (2018). The winter midlatitude-Arctic interaction: Effects of North Atlantic SST and high-latitude blocking on Arctic sea ice and Eurasian cooling. *Climate Dynamics*, *2018*. https://doi.org/10.1007/s00382-018-4301-5

Luo, B., Luo, D., Wu, L., Luo, D., Wu, L., Zhong, L., & Simmonds, I. (2017). Atmospheric circulation patterns which promote winter Arctic sea ice decline. *Environmental Research Letters*, *12*(5), 054017. https://doi.org/10.1088/1748-9326/aa69d0

Luo, D., Chen, X., Dai, A., & Simmonds, I. (2018). Changes in atmospheric blocking circulations linked with winter Arctic warming: A new perspective. *Journal of Climate*, *31*(18), 7661–7678. https://doi.org/10.1175/JCLI-D-18-0040.1

Majda, A. J., Franzke, C. L., Fischer, A., & Crommelin, D. T. (2006). Distinct metastable atmospheric regimes despite nearly Gaussian statistics: A paradigm model. *Proceedings of the National Academy of Sciences*, *103*(22), 8309–8314. https://doi.org/10.1073/pnas.0602641103

Mori, M., Watanabe, M., Shiogama, H., Inoue, J., & Kimoto, M. (2014). Robust Arctic sea-ice influence on the frequent Eurasian cold winters in past decades. *Nature Geoscience*, *7*(12), 869–873. https://doi.org/10.1038/ngeo2277

Nakamura, T., Yamazaki, K., Iwamoto, K., Honda, M., Miyoshi, Y., Ogawa, Y., & Ukita, J. (2015). A negative phase shift of the winter AO/NAO due to the recent Arctic sea-ice reduction in late autumn. *Journal of Geophysical Research: Atmospheres*, *120*, 3209–3227. https://doi.org/10.1002/2014JD022848

Neale, R. B., Jadwiga H. Richter, Andrew J. Conley, Sungsu Park, Peter H. Lauritzen, Andrew Gettelman, David L. Williamson (2010), Description of the NCAR Community Atmosphere Model (CAM4.0) (NCAR Tech. Note NCAR/TN-485+STR, 212 pp). Retrieved from http://www.cesm.ucar.edu/models/ccsm4.0/cam/docs/description/cam4_desc.pdf)

Overland, J. E., & Wang, M. (2010). Large-scale atmospheric circulation changes are associated with the recent loss of Arctic sea ice. *Tellus*, *62*(1), 1–9. https://doi.org/10.1111/j.1600-0870.2009.00421.x

Pavol, S. (2014). *Siberian global warming meets lukewarm reaction in Russia*. Rome Italy: Inter Press Service. Retrieved May 26, 2018, http://www.ipsnews.net/2014/06/siberian-global-warming-meets-lukewarm-reaction-in-russia/

Rayner, N. A., Parker, D. E., Horton, E. B., Folland, C. K., Alexander, L. V., Rowell, D. P., et al. (2003). Global analyses of sea surface temperature, sea ice, and night marine air temperature since the late nineteenth century. *Journal of Geophysical Research*, *108*(D14), 4407. https://doi.org/10.1029/2002JD002670

Screen, J. A., Deser, C., & Simmonds, I. (2012). Local and remote controls on observed Arctic warming. *Geophysical Research Letters*, *39*, L10709. https://doi.org/10.1029/2012GL051598

Screen, J. A., Deser, C., & Simmonds, I. (2014). Atmospheric impacts of Arctic sea-ice loss, 1979–2009: Separating forced change from atmospheric internal variability. *Climate Dynamics*, *43*(1-2), 333–344. https://doi.org/10.1007/s00382-013-1830-9

Screen, J. A., & Simmonds, I. (2012). Declining summer snowfall in the Arctic: Causes, impacts and feedbacks. *Climate Dynamics*, *2012*(38), 2243–2256.

Screen, J. A., Simmonds, I., Deser, C., & Tomas, R. (2013). The atmospheric response to three decades of observed Arctic sea ice loss. *Journal of Climate*, *26*(4), 1230–1248. https://doi.org/10.1175/JCLI-D-12-00063.1

Shepherd, T. G. (2014). Atmospheric circulation as a source of uncertainty in climate change projections. *Nature Geoscience*, *7*(10), 703–708. https://doi.org/10.1038/ngeo2253

Simmonds, I. (2018). What causes extreme hot days in Europe? *Environmental Research Letters*, *13*(7), 071001. https://doi.org/10.1088/1748-9326/aacc78

Simmonds, I., & Govekar, P. D. (2014). What are the physical links between Arctic sea ice loss and Eurasian winter climate? *Environmental Research Letters*, *9*(10), 101003. https://doi.org/10.1088/1748-9326/9/10/101003

Sura, P., & Hannachi, A. (2015). Perspectives of non-Gaussianity in atmospheric synoptic and low-frequency variability. *Journal of Climate*, *28*(13), 5091–5114. https://doi.org/10.1175/JCLI-D-14-00572.1

Xie, J., & Zhang, M. (2017). Role of internal atmospheric variability in the 2015 extreme winter climate over the North American continent. *Geophysical Research Letters*, *44*, 2464–2471. https://doi.org/10.1002/2017GL072772

Yang, X., Yuan, X., & Ting, M. (2016). Dynamical link between the Barents–Kara Sea ice and the Arctic oscillation. *Journal of Climate*, *29*(14), 5103–5122. https://doi.org/10.1175/JCLI-D-15-0669.1